Geophys. J. Int. (1995) **122,** 183–194

Statistical test of the tidal triggering of earthquakes: contribution of the ocean tide loading effect

Hiroshi Tsuruoka, Masakazu Ohtake and Haruo Sato

Geophysical Institute, Faculty of Science, Tohoku University, Aoba-ku, Sendai 980-77, Japan

Accepted 1995 January 6. Received 1995 January 5; in original form 1994 June 1

SUMMARY

The possibility of tidal triggering of earthquakes is investigated for a data set that contains 988 globally distributed earthquakes with magnitude of 6.0 or larger. We synthesize the theoretical time history of tidal stress change, including both solid earth tide and ocean tide loading, at the earthquake hypocentre, and assign the phase angle of tidal stress at the occurrence time of each earthquake. The stress due to ocean loading is obtained by convolving the global ocean tide distribution by Schwiderski with the Green's functions for surface point-mass load, which were newly computed for the Preliminary Earth Model of Dziewonski & Anderson. By testing the distribution of the phase angle statistically, we found a significant phase selectivity for normal-fault-type earthquakes; the null hypothesis that earthquakes take place randomly irrespective of the phase angle is rejected at the significance level of 0.54 per cent for the cubic stress component (trace of the tidal stress tensor), and 0.58 per cent for the stress component along the tension axis of the earthquake's focal mechanism. The highest population of normal-fault-type earthquakes appears at the time of maximum extensional stress, implying that a decrease in the confining pressure due to the earth tide is responsible for triggering earthquake occurrence. Such a clear phase selectivity is not seen for strike-slip- and thrust-type earthquakes. The fault-type dependence of the earthquake triggering effect suggests that shear stress change on the fault plane is also an essential factor of tidal triggering of earthquakes.

Key words: CMT catalogue, normal fault, ocean tide loading, PREM model, statistical test, tidal triggering.

1 INTRODUCTION

Many studies in the past have suggested that a small increase in crustal stress may trigger an earthquake when the stress in the focal region is at a critical state. Among the several kinds of potential trigger factors including atmospheric pressure, rainfall and ocean tide, the earth tide due to the traction of the moon and Sun has been of special concern as summarized by Aki (1956) and Tanaka (1985). The stress change due to the solid earth tide, less than 3×10^3 Pa (30 mbar) at the surface, is much smaller than the stress drop associated with earthquake occurrence. The rate of stress change due to the earth tide, however, is equal to or greater than that of tectonic stress accumulation, and the tidal stress may control the occurrence time of an earthquake to some extent.

Indeed, there are many studies that have reported a positive correlation between the earth tide and earthquake occurrence (e.g. Shlien 1972; Nagasawa 1973; Heaton 1975; Sauck 1975; Klein 1976; Hamada 1978; Shimada 1978; Souriau, Souriau & Gagnepain 1982; Ding, Jia & Wang 1983; Kilston & Knopoff 1983; Oike & Taniguchi 1988; Rydelek, Davis & Koyanagi 1988; Lopes *et al.* 1990; Mitsunami & Yamasaki 1990) as well as correlation with volcanic eruptions (e.g. Mauk & Johnston 1973; Dzurisin 1980; McNutt & Beavan 1984). On the other hand, negative results have also been reported (e.g. Knopoff 1964; Shlien & Toksöz 1970; Heaton 1982; Rydelek, Sacks & Scarpa 1992). Although most parts of these studies focused on the seismicity in a rather small area of local to regional scale, a few papers (Heaton 1975, 1982; Ding *et al.* 1983; Lopes *et al.* 1990) analysed global earthquake data. The components compared with earthquake occurrence time were varied:

tidal stress, strain, gravity, potential, and celestial position of the moon and the Sun.

To investigate the correlation between the earth tide and earthquake occurrence, we should take the points listed below into consideration. The first and most important point of all is the effect of ocean tide loading, which was not properly incorporated in earlier studies. The loading effect is computed by convolving the Green's functions for a surface point load with global ocean tide distribution (Longman 1962, 1963; Farrell 1972; Scherneck 1990, 1991; Pagiatakis 1990), and an analysis including the ocean loading was performed in a few of the studies (Sauck 1975; Klein 1976; Shimada 1978; Souriau *et al.* 1982; McNutt & Beavan 1984). Those studies, however, used the Green's functions at the Earth's surface, and the response at the depth of earthquake occurrence was not properly evaluated. The amplitude of stress change due to the ocean tide is of order comparable to that due to the direct solid tide beneath and around oceanic basins, and neglecting the ocean tide loading effect will bring about an erroneous conclusion. The second point is the depth dependence of the earth tide. Heaton (1975, 1982) and Ding *et al.* (1983) synthesized theoretical tidal stress at earthquake depth for a comparison with earthquake occurrence time, although the computation was limited to the solid tide. In contrast, all the other studies used tidal components at the Earth's surface. However, the tidal stress should be computed at the depth of the hypocentre, since tidal stress depends on the depth in the oceanic region in particular, and the depth effect cannot be neglected. The third point is the completeness of the tidal constituents. Some earlier studies paid attention only to semi-diurnal components such as M2 and S2. They are actually dominant constituents, but diurnal components such as O1 and K1 are also of comparable importance particularly at high and middle latitudes. Since the time history of the earth tide is very complicated, we should use a reliable synthetic tide including higher order *constituents* for a comparison with earthquake occurrence time. Lastly, we emphasize the importance of considering the focal mechanism in analysis. Some earlier studies examined the correlation between earthquake occurrence time and change in tidal potential (Knopoff 1964; Shlien & Toksöz 1970; Shlien 1972), but the time history of the tidal potential is different from that of stress or strain. The same tidal stress tensor can act either positively or negatively to accelerate shear faulting, depending on the focal mechanism of the pending earthquake. Therefore, an analysis disregarding the focal mechanism will contribute little to our understanding of the physical mechanism of tidal triggering of earthquakes.

In the present study, we investigate a correlation between the earth tide and earthquake occurrence taking the above four points into consideration. Of particular importance is the synthesis of time series of theoretical tidal stress including both *solid earth tide* and the effect of ocean tide loading. Based on the synthetic time series, we examine statistically the possibility of tidal triggering for world earthquakes with surface magnitude equal to or larger than 6.0. Many of the earlier studies used the earth tide potential or tidal strain to examine the relation with earthquake occurrence time, but we use stress components since the stress change is physically the most fundamental factor in earthquake occurrence.

2 THEORETICAL TIDAL STRESS

2.1 Formulation

The elastic deformation of the Earth has two modes: spheroidal and toroidal. Tidal force, as well as surface mass loads produce only the spheroidal mode of deformation. Here, we assume that the Earth is spherically symmetric, non-rotating, elastic and isotropic. Spheroidal deformation of such a model is formulated by using $y_i (i = 1, 2, \ldots, 6)$ that satisfy a set of six differential equations (Alterman, Jarosch & Pekeris 1959; Takeuchi & Saito 1972):

$$\frac{dy_i(r, n)}{dr} = \sum_{j=1}^{6} a_{ij}[\rho(r), \lambda(r), \mu(r), g(r); r, n]\, y_j(r, n), \tag{1}$$

where $y_i(r, n)$ is a function of radius r for the nth mode, ρ is mass density, λ and μ are Lame's coefficients and g is the acceleration due to gravity. The explicit expression for matrix a_{ij} is given by eq. (82) of Takeuchi & Saito (1972). Displacement (u_r, u_θ, u_ϕ), stress $(\sigma_{rr}, \sigma_{r\theta}, \sigma_{r\phi})$ and potential V in spherical coordinates (r, θ, ϕ) are written using products of y_i and spherical harmonic functions $Y_n^m(\theta, \phi)$ of modes (n, m):

$$\begin{aligned}
u_r(r, \theta, \phi) &= \sum_{n,m} [y_1(r, n)\, Y_n^m(\theta, \phi)], \\
u_\theta(r, \theta, \phi) &= \sum_{n,m} \left[y_3(r, n) \frac{\partial Y_n^m(\theta, \phi)}{\partial \theta}\right], \\
u_\phi(r, \theta, \phi) &= \sum_{n,m} \left[y_3(r, n) \frac{1}{\sin\theta} \frac{\partial Y_n^m(\theta, \phi)}{\partial \phi}\right], \\
\sigma_{rr}(r, \theta, \phi) &= \sum_{n,m} [y_1(r, n)\, Y_n^m(\theta, \phi)], \\
\sigma_{r\theta}(r, \theta, \phi) &= \sum_{n,m} \left[y_4(r, n) \frac{\partial Y_n^m(\theta, \phi)}{\partial \theta}\right], \\
\sigma_{r\phi}(r, \theta, \phi) &= \sum_{n,m} \left[y_4(r, n) \frac{1}{\sin\theta} \frac{\partial Y_n^m(\theta, \phi)}{\partial \phi}\right], \\
V(r, \theta, \phi) &= \sum_{n,m} [y_5(r, n)\, Y_n^m(\theta, \phi)], \\
y_6(r, n) &= \frac{dy_5(r, n)}{dr} - 4\pi G\rho y_1(r, n) + \frac{n+1}{r} y_5(r, n),
\end{aligned} \tag{2}$$

where G is the universal gravitational constant, θ and ϕ are colatitude and easterly longitude, respectively.

The boundary conditions are

$$y_2 = -\frac{2n+1}{a} \frac{g(a)}{4\pi G} \sigma', \qquad y_4 = 0, \qquad y_6 = \frac{2n+1}{a} \tag{3}$$

on the Earth's surface $(r = a)$, where $\sigma' = 0$ for the solid tide and $\sigma' = 1$ for the surface load, and

$$y_1 = y_3 = y_5 = 0 \tag{4}$$

at the centre of the Earth.

All the y_is must be continuous at internal discontinuities, and all y_is except y_3 must be continuous at the core–mantle boundary. For the liquid core, we followed the formalism of Alterman *et al.* (1959) and Saito (1974).

We solved the system of equations (1) subject to the boundary conditions and the internal boundary conditions for the isotropic Preliminary Earth Model (PREM) of Dziewonski & Anderson (1981) with a slight modification: the top 3 km layer is replaced by a solid layer of $V_p = 5\,\mathrm{km\,s^{-1}}$, $V_s = 2.6\,\mathrm{km\,s^{-1}}$ and $\rho = 2.6\,\mathrm{g\,cm^{-3}}$. Hereafter, we refer to this modified earth model as the PREM model. We performed the integration by using the fourth-order Runge–Kutta method taking the step size in numerical integration as less than one-hundredth of a wavelength.

Figure 1 shows y_is for $n = 2$ computed for the solid ($\sigma' = 0$) and Fig. 2 shows y_is for $n = 2$ and 20 for surface mass load ($\sigma' = 1$). In order to examine the accuracy of the Runge–Kutta computation, we compared the result of y_is for upward integration from the centre to the surface of the Earth with the downward integration from the surface to the centre. The results are in good agreement, with the relative difference as small as of the order of 10^{-6}.

2.2 Solid tide

The tide-generating potential due to the attraction of the moon is represented as

$$W^1 = \sum_{n=2}^{\infty} W_n^1 = \frac{GM_1}{D_1} \sum_{n=2}^{\infty} \left(\frac{r}{D_1}\right)^n P_n(\cos\Psi), \tag{5}$$

$$\cos\Psi = \cos\theta\cos\delta + \sin\theta\sin\delta\cos(\phi - \alpha), \tag{6}$$

at the point (r, θ, ϕ), where r is radius from the Earth's centre, θ is colatitude and ϕ is easterly longitude. Other notations used here are as follows: M_1, mass of the moon; D_1, distance between the centre of the Earth and the moon; δ and α, codeclination and right ascension of the moon; P_n, Legendre polynomials. A similar expression applies to the Sun for potential W^2. The radial, colatitudinal and longitudinal displacements caused by the tide-generating potential are given by

$$\begin{aligned} u_r^s(r,\theta,\phi) &= \sum_{n=2}^{3}\sum_{j=1}^{2} y_1(r,n) W_n^j, \\ u_\theta^s(r,\theta,\phi) &= \sum_{n=2}^{3}\sum_{j=1}^{2} y_3(r,n) \frac{\partial W_n^j}{\partial\theta}, \\ u_\phi^s(r,\theta,\phi) &= \sum_{n=2}^{3}\sum_{j=1}^{2} y_3(r,n) \frac{\partial W_n^j}{\sin\theta\,\partial\theta}, \end{aligned} \tag{7}$$

where the suffix j indicates the moon ($j = 1$) or the Sun ($j = 2$). W_n^j corresponds to Y_n^m in eq. (2). It is sufficient to sum the above terms up to $n = 3$, since a/D is as small as 2×10^{-2} for the moon and 4×10^{-5} for the Sun. y_is for the solid tide are shown in Fig. 1. We can derive the tidal stress components from the tide-generating potential and its derivatives, by replacing $Y_n^m(\theta, \phi)$ in eq. (2) by $W_n^1 + W_n^2$.

2.3 Ocean loading

Elastic response of the solid earth to the ocean load is obtained by convolution of seawater mass distribution with Green's functions for displacement, strain and stress due to a point unit mass loading on the solid surface of the PREM model. The potential due to a unit point surface mass loading is written by the infinite sum of Legendre functions:

$$\begin{aligned} S &= \sum_{n=0}^{\infty} \frac{(2n+1)}{4\pi a^2} P_n(\cos\Theta) \\ &= \frac{ag(a)}{m_e}\left[\sum_{n=0}^{\infty} \frac{(2n+1)}{4\pi G a} P_n(\cos\Theta)\right], \end{aligned} \tag{8}$$

where m_e is the mass of the Earth and Θ is the angular

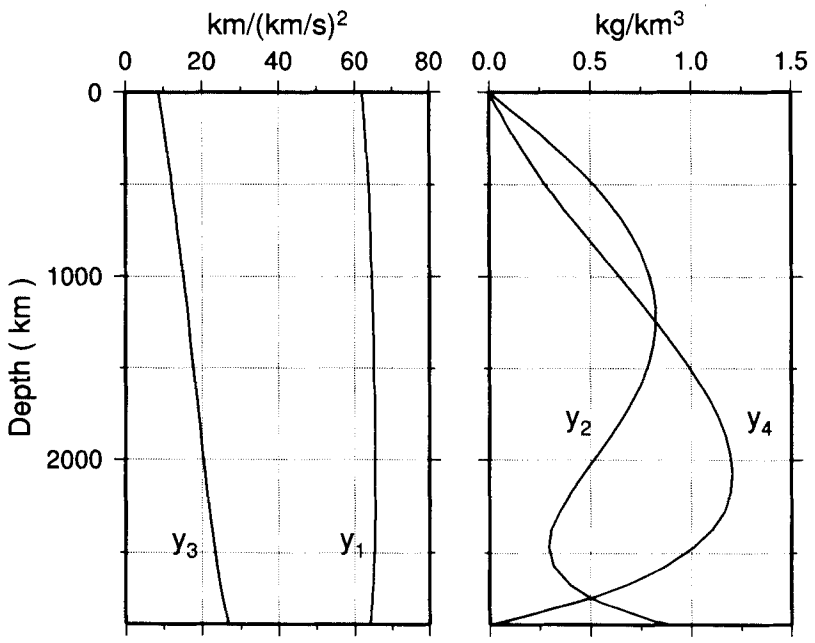

Figure 1. Depth dependence of $y_i(r, 2)$ for the solid earth tide for the PREM earth model.

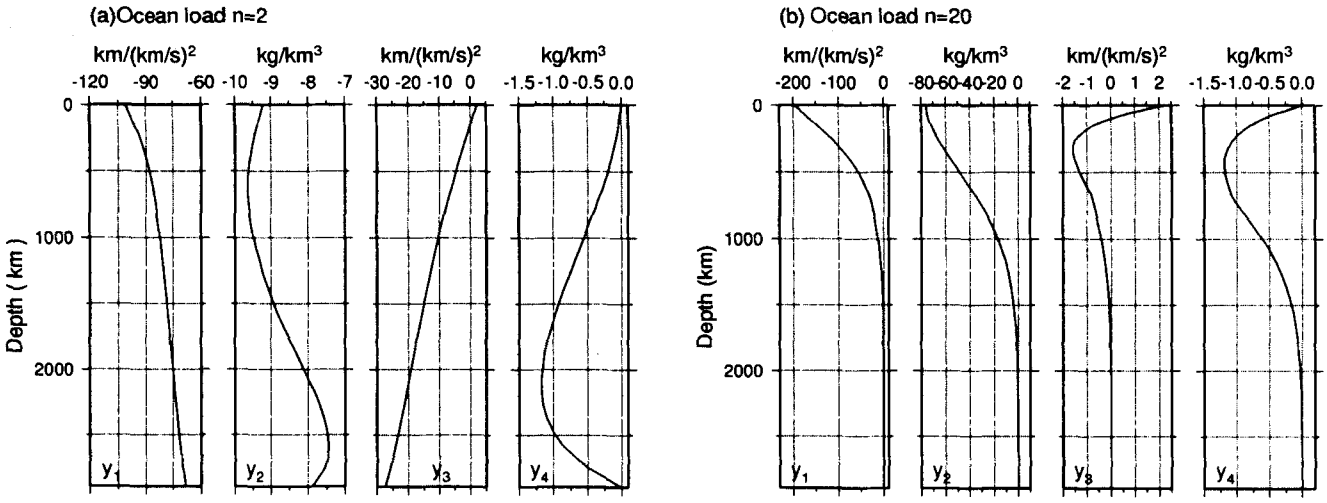

Figure 2. (a) Depth dependence of $y_i(r, 2)$ for the surface mass load for the PREM earth model. (b) Depth dependence of $y_i(r, 20)$.

distance from the loading point. Non-zero components of displacement and stress at radius r, and angular distance Θ are

$$
\begin{aligned}
u_r^{G}(r,\Theta) &= \frac{ag(a)}{m_e}\sum_{n=0}^{\infty} y_1'(r,n)P_n(\cos\Theta),\\
u_\Theta^{G}(R,\Theta) &= \frac{ag(a)}{m_e}\sum_{n=0}^{\infty} y_3'(r,n)\frac{\partial P_n(\cos\Theta)}{\partial\Theta},\\
\sigma_{rr}^{G}(r,\Theta) &= \frac{ag(a)}{m_e}\sum_{n=0}^{\infty} y_2'(r,n)P_n(\cos\Theta),\\
\sigma_{r\Theta}^{G}(r,\theta) &= \frac{ag(a)}{m_e}\sum_{m_e}^{\infty}\sum_{n=0}^{\infty} y_4'(r,n)\frac{\partial P_n(\cos\Theta)}{\partial\Theta},
\end{aligned}
\tag{9}
$$

where the superscript G denotes the Green's function. For the calculation of Green's functions, we summed the terms up to $n = 10\,000$, which secures a spatial resolution of less than 2 km. The Green's functions thus obtained are shown in Figs 3 and 4 for radial and tangential displacement, respectively. In these figures, the Green's functions are shown by normalizing by the reference Boussinesq solution at the surface of a homogeneous half-space (Farrell 1972). The normalizing function is

$$
u^*(a,\Theta) = -\frac{g(a)[\lambda(a)+2\mu(a)]}{4\pi\mu(a)[\lambda(a)+\mu(a)](a\Theta)} \tag{10}
$$

for radial displacement, and

$$
v^*(a,\Theta) = -\frac{g(a)}{4\pi[\lambda(a)+\mu(a)](a\Theta)} \tag{11}
$$

for tangential displacement. For the ocean tide distribution, we used Schwiderski's (1980) model, which is implemented with the computer program GOTIC by Sato & Hanada

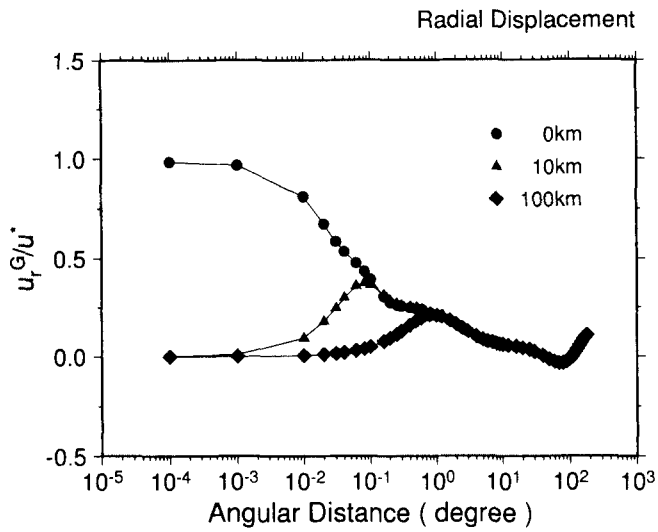

Figure 3. Vertical displacement Green's functions for a point mass load at depths of 0, 10 and 100 km. The Green's functions are shown by normalizing by the response of a half-space with $V_p = 5.0\,\mathrm{km\,s^{-1}}$, $V_s = 2.6\,\mathrm{km\,s^{-1}}$, $\rho = 2.6\,\mathrm{g\,cm^{-3}}$. See text for the normalizing function.

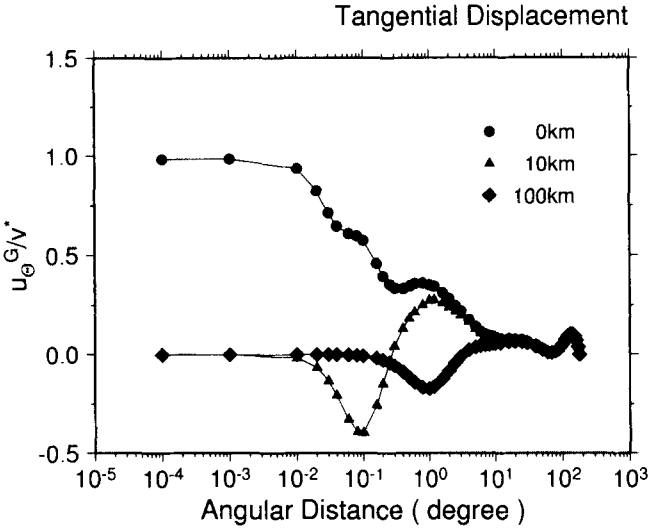

Figure 4. Tangential displacement Green's functions for a point mass load at depths of 0, 10 and 100 km. The Green's functions are shown by normalizing by the response of a half-space with $V_p = 5.0\,\mathrm{km\,s^{-1}}$, $V_s = 2.6\,\mathrm{km\,s^{-1}}$, $\rho = 2.6\,\mathrm{g\,cm^{-3}}$. See text for the normalizing function.

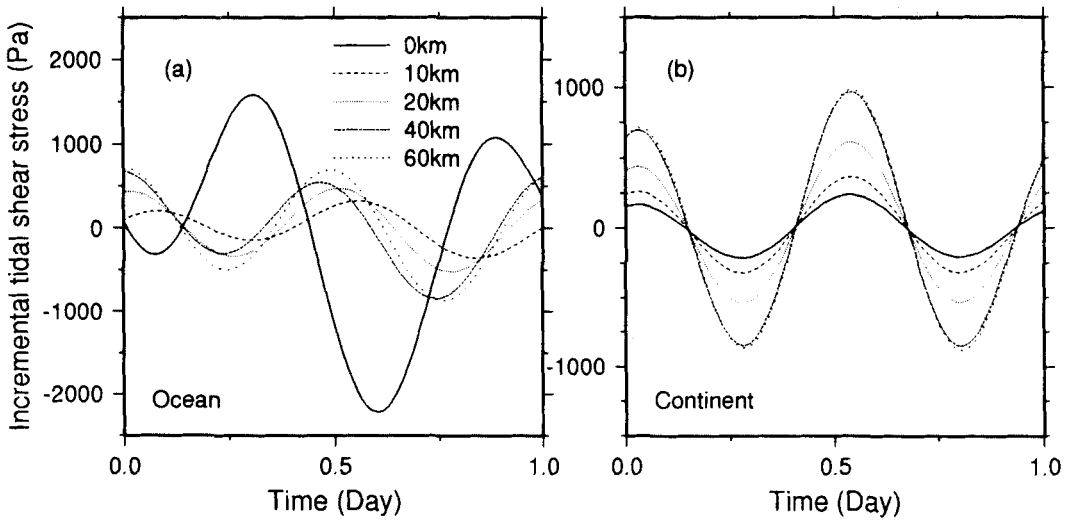

Figure 5. (a) Time history of the tidal shear stress of the oceanic earthquake at depths of 0, 10, 20, 40 and 60 km, where the epicentre is at 143.08° E, 39.95° N, and the fault geometry is set as strike = 135°, dip = 15° and rake is 90°. The stress history spans one day from 1989 November 1 (GMT). (b) Time history of the tidal shear stress of the continental earthquake at depths of 0, 10, 20, 40 and 60 km, where the epicentre is at 121.23° E, 57.03° N, and the fault geometry is set as strike = 6°, dip = 56° and rake is 170°. The stress history spans one day from 1989 April 20 (GMT).

(1984). This ocean tide model involves nine main constituents: M2, S2, K2, N2, O1, K1, P1, Q1 and Mf. Although the Green's functions at the Earth's surface were reported in Farrell (1972), we present here a complete set of the depth-dependent values. To compute the elastic response of the Earth, oceanic regions are divided into rectangular cells of $1° \times 1°$ for $\Theta > 7°$ and $7.5' \times 5'$ for $\Theta \leq 7°$.

Figure 5 is an example that compares the tidal stress change at depths of 0, 10, 20, 40 and 60 km for an oceanic earthquake (a) and for a continental earthquake (b). As we investigate the correlation between tidal stress and earthquake occurrence based on the phase-angle analysis, Fig. 5(a) shows that use of the tidal stress components at the Earth's surface may lead us to an erroneous conclusion for oceanic region earthquakes in particular.

3 STATISTICAL TEST

We examine statistically whether incremental tidal stress may trigger earthquakes or not, based on phase-angle analysis as performed by Shlien (1972), Heaton (1975, 1982) and other researchers. The method is as follows. First, we compute tidal stress components, including both the solid earth tide and ocean tide loading, at the location of the hypocentre, following the procedure described in the previous section. The phase angle at the time of earthquake occurrence is assigned with reference to the time history of stress change.

Figure 6 illustrates how to assign the phase angle. Picking up the stress peak nearest to the earthquake occurrence time, we assign a phase angle of 0° to the peak, and ±180° to the following and preceding troughs, respectively. The time interval between a tidal peak and adjacent trough is not constant, and such a phase-based analysis permits a uniform comparison of data, regardless of the asymmetry of tidal stress history.

Based on the phase angle thus defined, we test whether earthquakes take place around a certain phase angle or not by using Schuster's test (e.g. Heaton 1975). The basic parameter for the test is R:

$$R = \sqrt{A^2 + B^2}, \tag{12}$$

$$A = \sum_{i=1}^{N} \cos \psi_i, \qquad B = \sum_{i=1}^{N} \sin \psi_i, \tag{13}$$

where ψ_i is the phase angle of the ith earthquake and N is the total number of earthquakes. If earthquakes take place randomly, independent of tidal phase, A and B distribute around zero mean with a variance of $N/2$, and R^2 obeys the χ^2 distribution with two degrees of freedom similar to the 2-D random walk. The probability that R or a larger value occurs by chance is

$$p = \exp\left(-\frac{R^2}{N}\right) \tag{14}$$

when N is large enough (larger than 10). The parameter

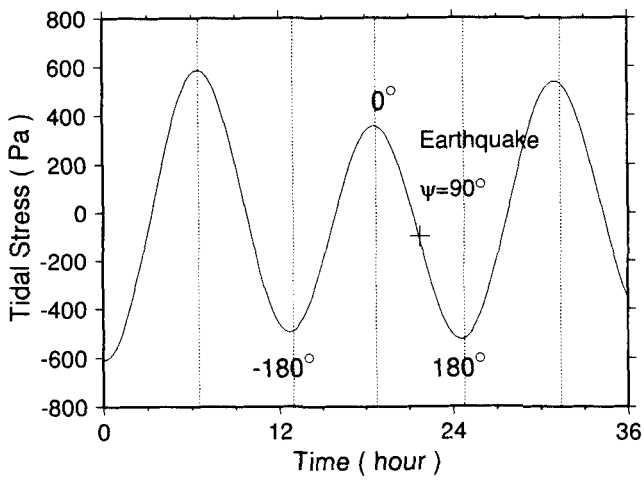

Figure 6. Definition of a tidal phase angle; the peak and troughs of the stress history are assigned to 0° and ±180°, respectively.

p represents the significance level to reject the null hypothesis that earthquakes occur randomly with respect to the tidal phase angle. As the parameter p becomes smaller, the confidence in rejecting the null hypothesis becomes higher. We test the selectivity of tidal phase of earthquake occurrence based on the p value.

4 DATA

We analysed 988 earthquakes of $M_s \geq 6.0$ listed in the Harvard centroid-moment tensor (CMT) catalog for the period from 1977 January 1 to 1992 June 30. The CMT catalog was obtained by accessing the data file of Harvard University directly through a computer net. To minimize the possible distortion of a data set by aftershocks, smaller earthquakes are excluded from the analysis. The focal parameters we used are those for the best-fitting double-couple solutions. The epicentres and focal depths of earthquakes were also taken from the Harvard catalog that provides the centroid locations. It is not appropriate in our analysis to use the focal depth of the preliminary determination of earthquakes since the depths of many shallow earthquakes are constrained at the normal depth, 33 km.

Figure 7 shows the epicentres and depth distribution of earthquakes that are used in this study. As shown in the figure, many hypocentres are located in or near the oceanic region; therefore, careful treatment of the ocean tide loading effect is needed for a reliable analysis of tidal triggering of earthquakes.

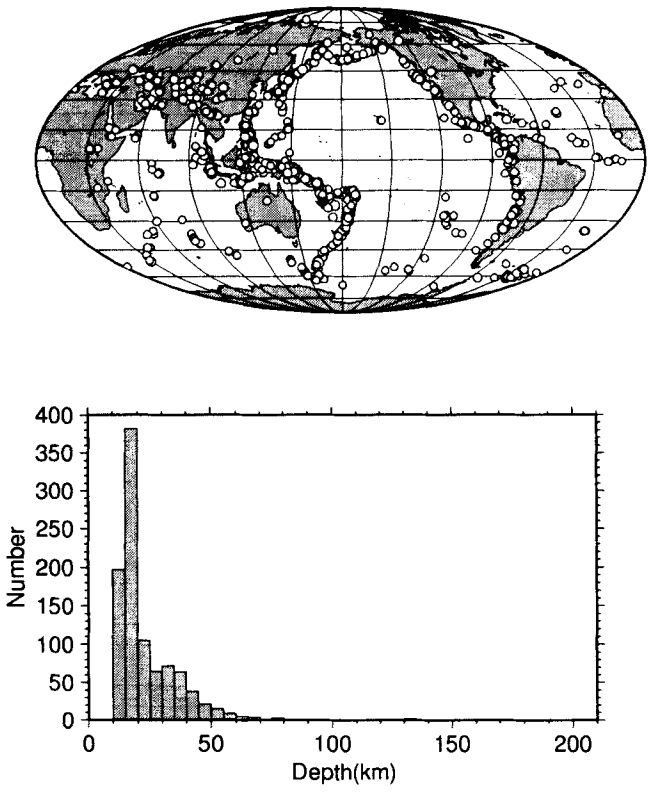

Figure 7. Epicentre distribution of 988 earthquakes used in the analysis (top), and a histogram of the focal depth distribution (bottom).

5 ANALYSIS AND RESULTS

Among the incremental stress components due to the earth tide, shear stress and normal stress on the fault plane are of greatest interest. The normal stress, however, is not uniquely estimated, since the fault plane and auxiliary plane are not discriminated from the focal mechanism solution. On the other hand, the shear stress can be resolved since it takes the same value both for the fault plane and auxiliary plane due to the symmetrical nature of the stress tensor. Thus we investigated the change in the shear stress on the fault plane, as well as orthogonal stress components along-the-principal axis (pressure, null and tension axes), of the earthquake focal mechanism. The cubic stress change, defined by the trace of the incremental stress tensor, represents the change of confining stress in the focal region. We note that it is the invariant quantity of the stress tensor. The unit vectors $(\mathbf{e}_1, \mathbf{e}_2, \mathbf{e}_3)$ are defined by along-the-tension, null and pressure stress axes, respectively, which can be calculated from the focal mechanism solution. We also calculate along-the-principal-axis stress components as follows:

$$\sigma_T = 2\mu\varepsilon_{11}, \qquad \sigma_N = 2\mu\varepsilon_{22}, \qquad \sigma_P = 2\mu\varepsilon_{33}, \tag{15}$$

where ε_{11}, ε_{22} and ε_{33} are strain tensor components for this coordinate. As stated above, for along-the-principal-axis stress components, we calculated the values in which the confining pressure change is removed. All the stress components are defined positive for extensional stress so that the phase angles of 0° and 180° denote the maximum extensional stress and maximum compressional stress, respectively.

We computed the phase angle at the origin time of each earthquake for the five stress components described above. Fig. 8 shows the frequency distribution of the phase angle for each of the stress components; the data set includes all 988 earthquakes. The results of Schuster's test are also shown by parameter p at the top right of each figure. The distribution of tidal phase is nearly uniform for all of the stress components, and does not show any phase selectivity. The p values ranging from 12 to 91 per cent are too large to reject the null hypothesis that earthquakes occur randomly irrespective of tidal phase. Thus, a correlation between the earth tide and earthquake occurrence is not seen for the data set including all the earthquakes.

Next, we conduct a similar statistical test by dividing the earthquakes into four fault types: normal, thrust, strike-slip and oblique-slip faults. The classification of fault type is given in Table 1. We here follow the definition of the fault orientation parameters of Aki & Richards (1980). Fig. 9 shows the result for the cubic stress component. It can be clearly seen that earthquakes of normal fault type show a strong correlation ($p = 0.54$ per cent) with tidal stress in contrast to other fault types. The largest number of earthquakes of normal fault type are distributed around $\psi = 0°$, implying that the majority of earthquakes tend to occur at the time of maximum tensile stress. Figs 10–12 show the results for the stress components along-the-tension axis, null axis and pressure axis, respectively. In Fig. 10, a high correlation appears again for normal fault type earthquakes ($p = 0.58$ per cent), where the largest number

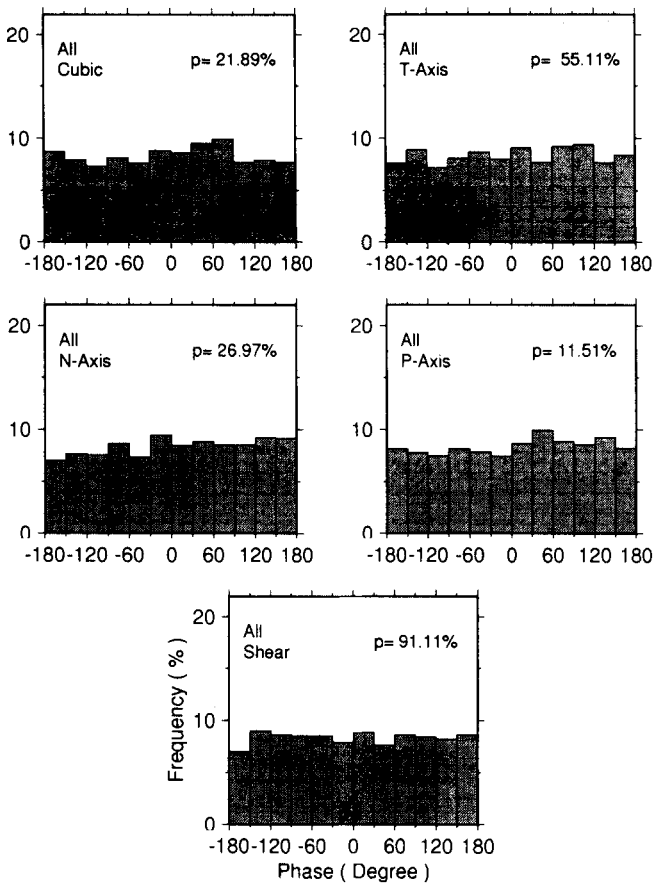

Figure 8. Frequency distribution of tidal phase angle at the time of earthquake occurrence for all earthquakes; the five panels are for different stress components. The parameter p of Schuster's test is shown in each panel.

of earthquakes distribute in the phase range of $\psi = 0°$–$60°$. Significant correlation is not seen for other fault types. For the null-axis and pressure-axis stress components, no correlation is found for any of the fault types (see Figs 11 and 12). Fig. 13 shows the results for the shear stress. A significant correlation is not found for any of the fault types. The smallest value of p is found for thrust type ($p = 3.1$ per cent), but this p value is marginal for rejecting the null hypothesis.

We further divided the normal-fault-type earthquakes into two categories: land region and oceanic region earthquakes, where land region earthquakes are those located on land more than 100 km from the nearest coast line. The p value for the cubic stress component is 64.1 per cent for the land region, but is as small as 0.64 per cent for the oceanic region.

Summarizing the results of the statistical analysis, we conclude that the tidal triggering effect occurs only for normal-fault-type earthquakes, in particular those occurring in the oceanic region. This effect is dominant in the change of cubic and along-the-tension-axis stress components, and normal-fault-type earthquakes tend to take place at the time of maximum extensional stress.

Table 1. Classification of fault types.

Fault Type	Slip Direction
Normal	$-120° \leq \mathrm{Rake} \leq -60°$
Thrust	$60° \leq \mathrm{Rake} \leq 120°$
Strike-Slip	$0° \leq \lvert\mathrm{Rake}\rvert \leq 30°, 150° \leq \lvert\mathrm{Rake}\rvert \leq 180°$
Oblique	$30° < \lvert\mathrm{Rake}\rvert < 60°, 120° < \lvert\mathrm{Rake}\rvert < 150°$

6 DISCUSSION

Our analysis revealed a significant correlation between the earth tide and earthquake occurrence by comparing the earthquake occurrence time with theoretical tidal stress. We emphasize that the effect of ocean tide loading at the depth of the hypocentre is properly incorporated for the first time in a study of this kind. Some earlier studies incorporated the effect of ocean tide loading (Sauck 1975; Klein 1976; Shimada 1978; Souriau *et al.* 1982; McNutt & Beavan 1984), but all of them assumed that the stress or strain change at the focal depth is the same as that at the Earth's surface.

Heaton (1982), investigating global earthquakes, obtained the negative result that the correlation between the earth tide and earthquake occurrence was not detected for any of the fault types. The contradiction with our result can hardly be attributed to potential regionality of the tidal triggering effect, since the spatial distribution of earthquakes used for the analysis is not much different. The essential difference is that the ocean tide loading effect is not considered by Heaton (1982). In Fig. 14, we show the frequency distribution of the tidal phase angle for the cubic stress, where the effect of ocean tide loading is neglected. The p value for the normal-fault-type earthquakes is as large as 11 per cent, and significant phase selectivity is not seen for any of the fault types, in good agreement with the conclusion of Heaton (1982). The clear contrast between Fig. 9 (ocean tide loading is incorporated) and Fig. 14 demonstrates the importance of the ocean tide loading effect in synthesizing theoretical tidal stress.

When earthquakes in a small region are dealt with, the neglect of ocean tide loading will not greatly affect the phase selectivity since the time lag of the ocean tide behind the direct solid tide is nearly constant. This may be a reason why tidal correlation is frequently reported for earthquakes in a small region in spite of the neglect of the ocean tide loading effect. We, however, note that the phase selected by such an analysis is not necessarily the true tidal phase, and care is needed in interpreting the physical mechanism of earthquake triggering.

Our analysis showed that the tidal triggering effect is found only for earthquakes of normal fault type. Why is the effect not evident for the other fault types? A plausible interpretation is the difference in the efficiency of tidal stress change in generating shear faulting. Based on Byerlee's friction law, Kibry (1980) proposed that the stress required to generate faulting is largest for thrust faults, smallest for normal faults, and intermediate for strike-slip faults. This model suggests that a small stress increase is most effective in generating faulting in the case of normal faults. The most dominant contribution of the ocean tide loading is an increase in the overburden pressure under the ocean. The increase in shear stress for strike-slip faults is small while it is large for dip-slip faults. Fig. 15 gives an example that compares the shear stress change on normal and strike-slip faults located in the same place. It is plausible that

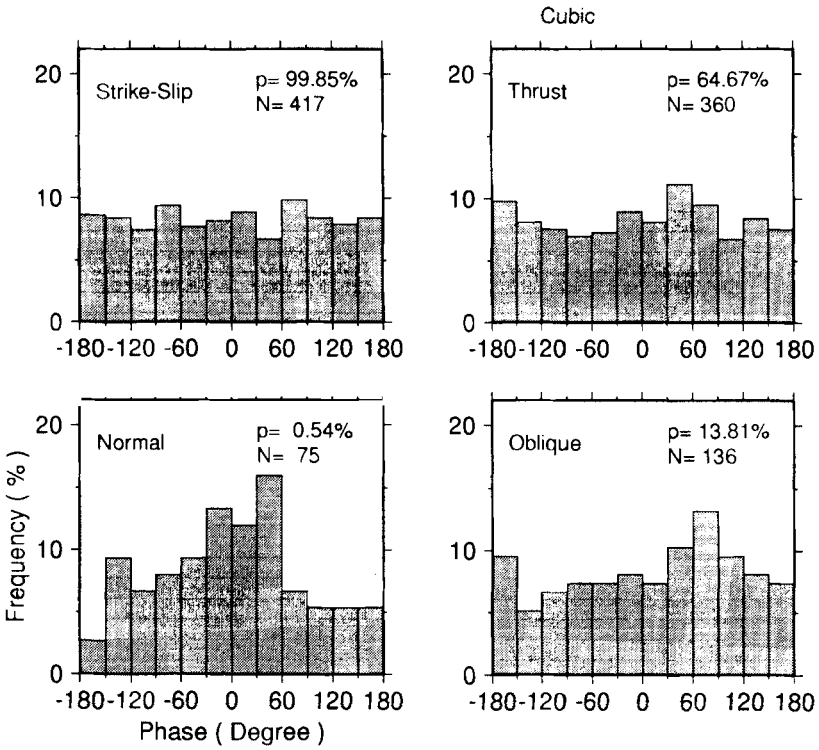

Figure 9. Frequency distribution of tidal phase angle at the time of earthquake occurrence for the cubic stress component; the four panels are for different fault types. The parameter p of Schuster's test is shown in each panel.

the distinct tidal triggering for the normal-fault-type earthquakes may be attributed to the larger shear stress change on the fault plane. A larger stress change is expected for the thrust fault, but the earthquake triggering efficiently will be lower than the normal fault type as was discussed above. A tidal correlation with earthquake occurrence was not detected for the shear stress on the fault plane (Fig. 13). The reason is not clear for the moment, but we suggest

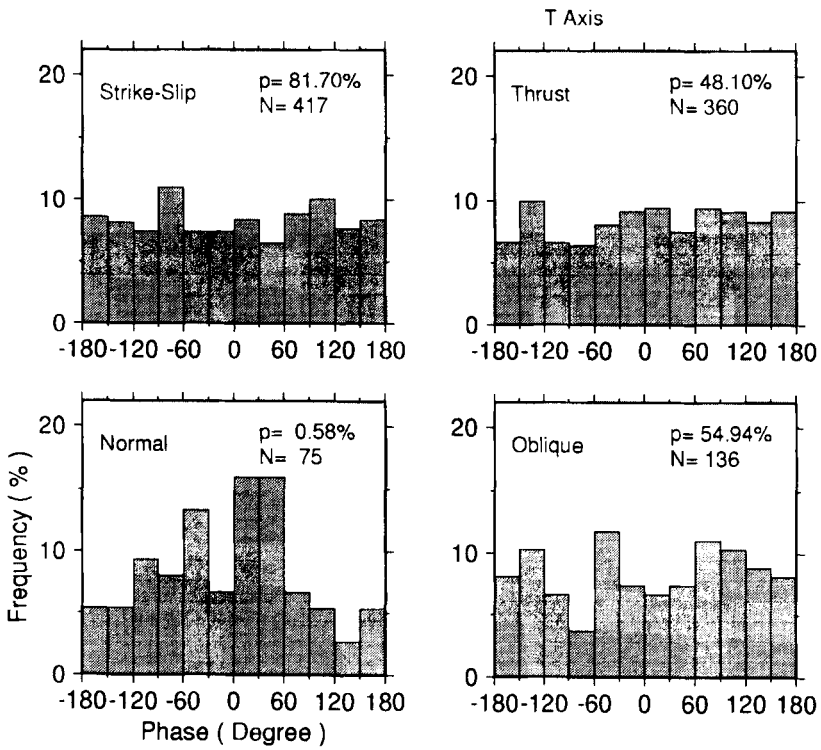

Figure 10. Frequency distribution of tidal phase angle at the time of earthquake occurrence for the along-the-tension-axis stress component; the four panels are for different fault types. The parameter p of Schuster's test is shown in each panel.

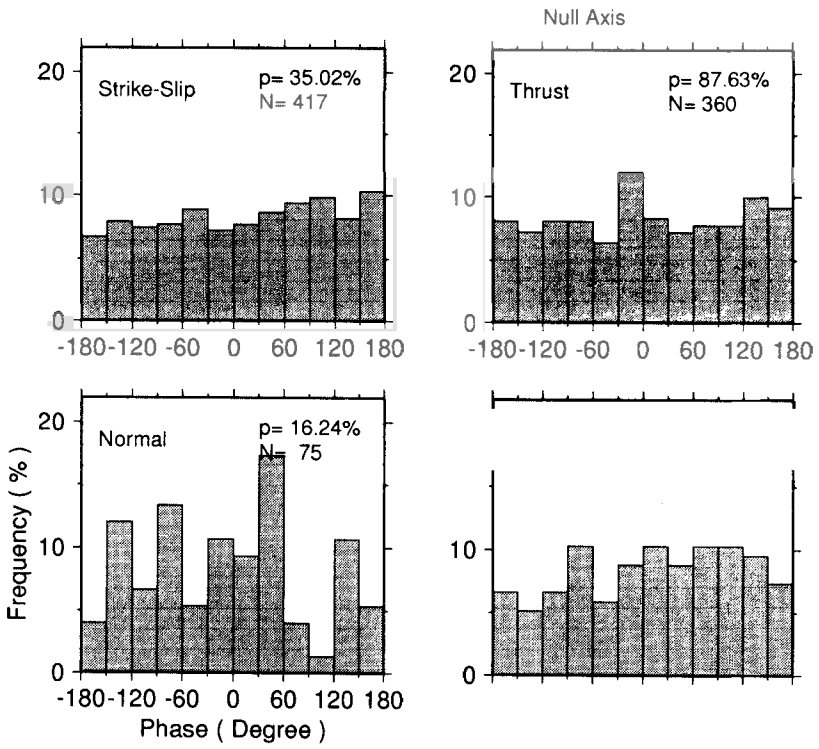

two possibilities: the difference in principal axis orientation between the earthquake-generating stress tensor and focal mechanism, and possible errors in the focal mechanism solution. These factors may seriously affect the result. On the other hand, a clear correlation was found for the cubic stress. We note that the cubic stress is an invariant quantity of the stress tensor, independent of rotation of the cordinate system, and is not affected by uncertainty of the fault

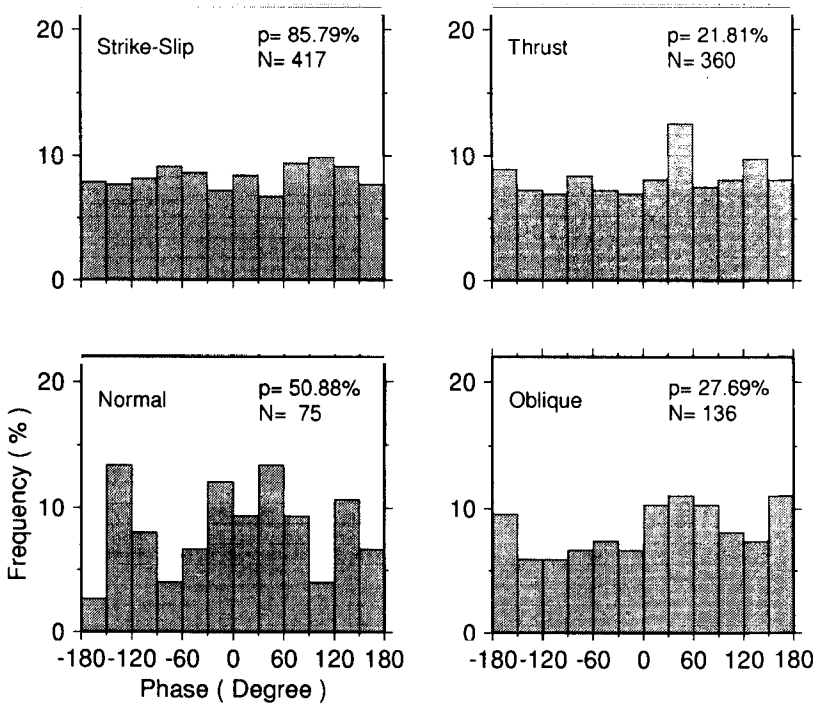

Figure 12. Frequency distribution of tidal phase angle at the time of earthquake occurrence for the along-the-pressure-axis stress component; the four panels are for different fault types. The parameter p of Schuster's test is shown in each panel.

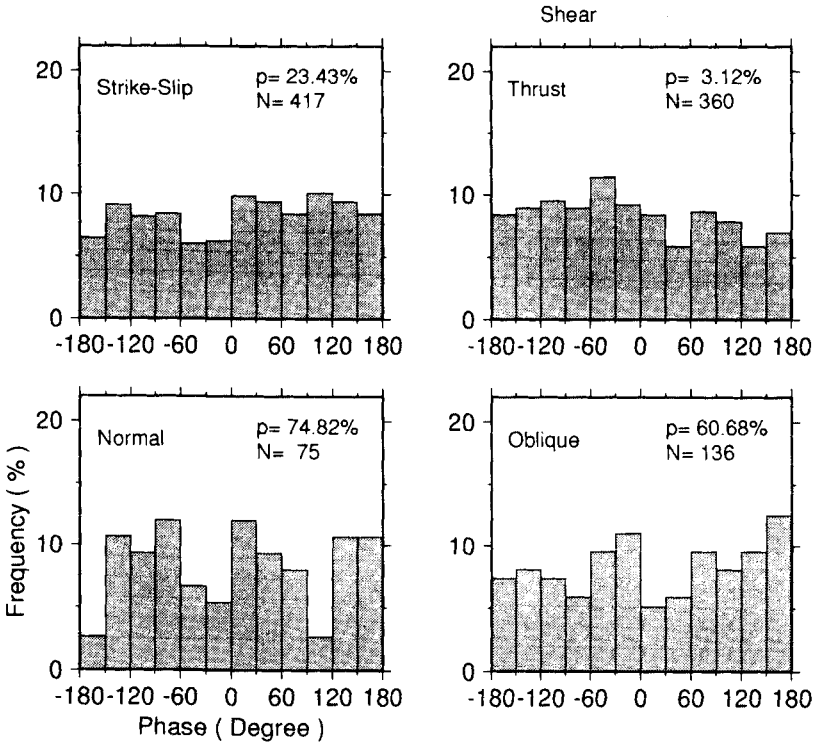

Figure 13. Frequency distribution of tidal phase angle at the time of earthquake occurrence for the shear stress component; the four panels are for different fault types. The parameter p of Schuster's test is shown in each panel.

plane. A complete set of stress components on the fault plane is needed to discuss further the physical mechanism of tidal triggering of earthquakes.

The present study focused on the tidal phase, but tidal amplitude may also be a key parameter of earthquake triggering as was suggested in the previous paragraph. We expect future studies to use data sets that include fault-plane information. It is also of great interest to clarify whether the

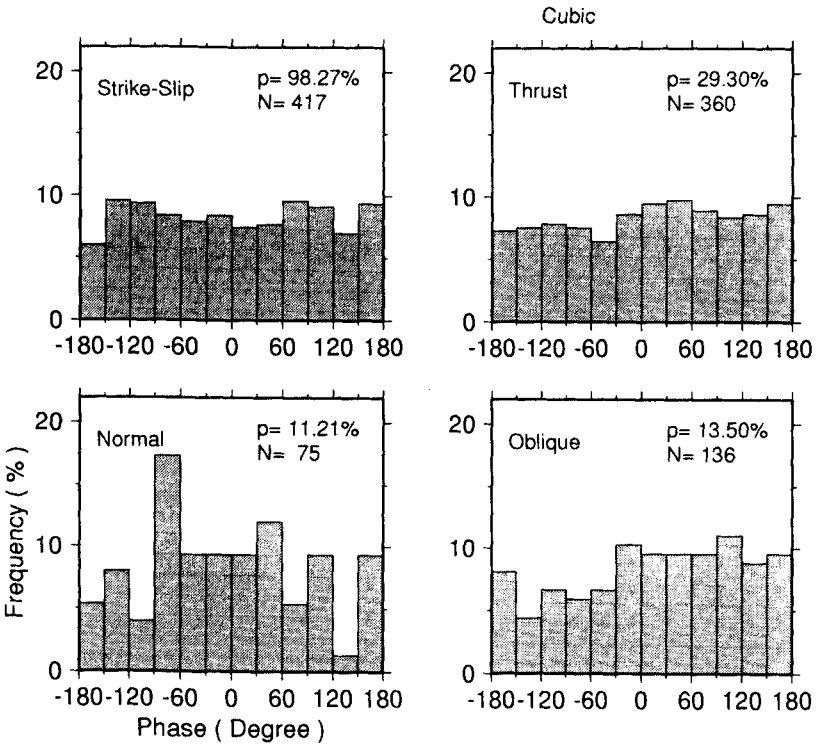

Figure 14. Frequency distribution of tidal phase angle at the time of earthquake occurrence for the cubic stress component due to solid tide only; the four panels are for different fault types. The parameter p of Schuster's test is shown in each panel.

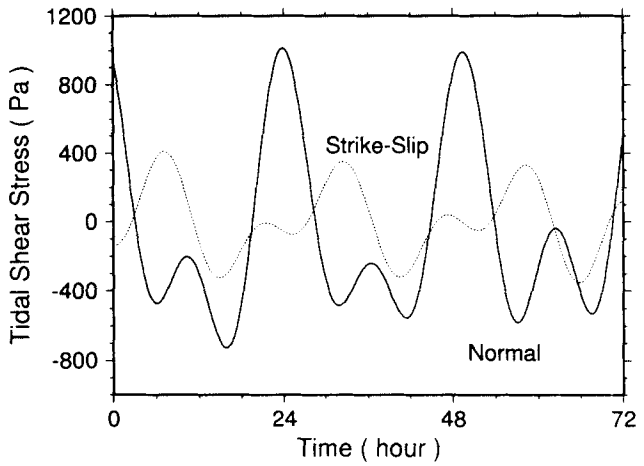

Figure 15. An example of the time history of the tidal shear stress on fault planes of normal type (solid curve), and strike-slip type (dotted curve) earthquakes. The hypocentre is at 72.4°E, 41.9°N, $H = 15$ km, and the fault geometry is set as strike = 90°, dip = 50°. The rake is −90° for the normal-fault-type, and 0° for the strike-slip type. The stress history spans 3 days from 1971 October 25 to 27 (GMT).

tidal triggering effect depends on earthquake size or not. Table 2 compares p values for the cubic stress for three subsets of earthquakes with different magnitude thresholds. We see a weak trend with the p value decreasing (correlation increases) with lower magnitude threshold for most of the fault types. This trend, however, is not conclusive for normal-fault-type earthquakes which exhibit significant correlation with tidal stress change. A data set covering a wider magnitude range is necessary to come to a final conclusion. The above investigation is limited to the homogeneous shell model. We note that the influence of local inhomogeneities such as geological structure and topography can have an additional influence on the stress distribution.

7 CONCLUSIONS

We have estimated theoretically the stress change due to the earth tide including both the solid earth tide and ocean tide loading effect at the depth of earthquake focus. Based on the theoretical tidal stress, we tested whether the time of earthquake occurrence correlates statistically with tidal stress or not by using Schuster's method. The data we used are 988 earthquakes with a surface-wave magnitude of 6.0 or larger that are listed in the Harvard centroid-moment tensor (CMT) catalog. The main results of this study are summarized as follows.

(1) Normal-fault-type earthquakes tend to occur at the time when the cubic tidal stress takes a maximum tensile value or a little bit later. The null hypothesis that earthquakes occur independently of tidal phase angle of cubic stress is rejected at a significance level as low as 0.54 per cent.

(2) The phase selectivity appears stronger for earthquakes in the oceanic region than those in the land region, suggesting the predominant effect of ocean tide loading.

(3) We do not find a correlation with tidal phase for the occurrence time of strike-slip- and thrust-type earthquakes.

These results indicate that earthquakes of normal fault type tend to be triggered by a small decrease in the compressional normal stress on the fault plane due to the earth tide. Our analysis did not show a clear correlation between earthquake occurrence and shear stress change on the fault plane. However, the absence of an apparent tidal triggering effect for the strike-slip and thrust-type earthquakes strongly suggests that the shear stress change is also an essential component of tidal triggering of earthquakes.

ACKNOWLEDGMENTS

We thank the scientist at Harvard University who provided us with CMT solutions through a computer net. We also thank T. Sato and H. Hanada for making available the global ocean tide distribution obtained by their computer program 'GOTIC'. We also wish to thank P. Wessel and W. H. F. Smith for offering us the plotting utility, GMT-SYSTEM.

REFERENCES

Aki, K., 1956. Some problems in statistical seismology, *Zisin II*, **8**, 205–208 (in Japanese).

Aki, K. & Richards, P.G., 1980. *Quantitative Seismology*, Vol. 1, W.H. Freeman and Co., San Francisco.

Alterman, Z., Jarosch, H. & Pekeris, C.L., 1959. Propagation of rayleigh waves in the earth, *Proc. R. Soc. Lond. A*, **252**, 80–95.

Ding, Z., Jia, J. & Wang, R., 1983. Seismic triggering effect of tidal stress, *Tectonophysics*, **93**, 319–335.

Dziewonski, A.M. & Anderson, D.L., 1981. Preliminary reference earth model, *Phys. Earth. planet. Inter.*, **25**, 297–356.

Dzurisin, D., 1980. Influence of fortnightly earth tides at Kilauea Volcano, Hawaii, *Geophys. Res. Lett.*, **7**, 925–928.

Farrell, W.E., 1972. Deformation of the earth by surface loads, *Rev. Geophys. Space Phys.*, **103**, 761–797.

Hamada, N., 1978. On the relation between earth tidal strain and Matsushiro earthquakes. *Q. J. seism.*, **43**, 1–10 (in Japanese).

Table 2. Significance level p of Schuster's test for the cubic stress for earthquake subsets of different magnitude ranges.

Category	$6.0 \leq M_s < 6.5$	$6.0 \leq M_s < 7.0$	$6.0 \leq M_s \leq 8.5$
Normal	2.74%(45)	0.16%(66)	0.54%(75)
Thrust	4.81%(198)	29.9%(299)	64.7%(360)
Strike-Slip	49.9%(277)	88.8%(377)	99.9%(417)
Oblique	9.57%(81)	8.82%(116)	13.8%(136)
All	1.41%(601)	2.54%(858)	21.9%(988)

Numerals in parentheses are the numbers of earthquakes included in the subset.

Heaton, T.H., 1975. Tidal triggeirng of earthquakes, *Geophys. J.R. astr. Soc.*, **43,** 307–326.

Heaton, T.H., 1982. Tidal triggering of earthquakes, *Bull. seism. Soc. Am.*, **72,** 2181–2200.

Kilston, S. & Knopoff, L., 1983. Lunar–solar periodicities of large earthquakes in southern California, *Nature*, **304,** 21–25.

Kirby, S., 1980. Tectonic stress in the lithosphere: Constraints provided by the experimental deformation of rock, *J. geophys. Res.*, **85,** 6353–6363.

Klein, F.W., 1976. Earthquake swarms and semidiurnal solid earth tide, *Geophys. J. R. astr. Soc.*, **45,** 245–295.

Knopoff, L., 1964. Earth tides as a triggering mechanism for earthquakes. *Bull. seism. Soc. Am.*, **54,** 1865–1870.

Longman, I.M., 1962. A green's function for determining the deformation of the earth under surface mass loads, 1, theory, *J. geophys. Res.*, **68,** 845–850.

Longman, I.M., 1963. A green's function for determining the deformation of the earth under surface mass loads, 2, computational and numerical results, *J. geophys. Res.*, **69,** 485–496.

Lopes, R.M.C., Malin, S.R.C., Mazzarella, A. & Palumbo, A., 1990. Lunar and solar triggering of earthquakes, *Phys. Earth. planet. Inter.*, **59,** 127–129.

Mauk, F.J. & Johnston, M.J.S., 1973. On the triggering of volcanic eruptions by earth tides, *J. geophys. Res.*, **78,** 3356–3362.

McNutt, S.R. & Beavan, R.J., 1984. Patterns of earthquakes and the effect of solid earth and ocean load tides at Mount St. Helens prior to the May 18, 1980, eruption, *J. geophys. Res.*, **89,** 3075–3086.

Mitsunami, T. & Yamasaki, Y., 1990. Tidal strain and earthquake occurrence, *Chikyu Monthly*, **12,** 369–378 (in Japanese).

Nagasawa, K., 1973. The correlation between the earthquake occurrence and positions of moon and sun—About the earthquakes in and near Japan, *J. geol. Soc. Japan*, **19,** 179–189 (in Japanese).

Oike, K. & Taniguchi, K., 1988. The relation between seismic activities and earth tides in the case of the Matsushiro earthquake swarm, *Bull. Disas. Prev. Res. Inst., Kyoto Univ.*, **38,** 17–28.

Pagiatakis, S.D., 1990. The response of a realistic earth to ocean tide loading, *Geophys. J. Int.*, **103,** 541–560.

Rydelek, P.A., Davis, P.M. & Koyanagi, R.Y., 1988. Tidal triggering of earthquake swarms at Kilauea volcano, Hawaii, *J. geophys. Res.*, **93,** 4401–4411.

Rydelek, P.A., Sacks, I.S. & Scarpa, R., 1992. On tidal triggering of earthquakes at Campi Flegrei, Italy, *Geophys. J. Int.*, **109,** 125–137.

Saito, M., 1974. Some problems of static deformation of the earth, *J. Phys. Earth*, **22,** 123–140.

Sato, T. & Hanada, H., 1984. A program for the computation of oceanic tidal loading effects 'GOTIC', *Publ. Int. Latitu. Mizusawa*, **18,** 63–82.

Sauck, W.A., 1975. The Brawley, California earthquake sequence of January, 1975, and triggering by earth tides, *Geophys. Res. Lett.*, **2,** 506–509.

Scherneck, H.G., 1990. Loading green's functions for a continental shield with a Q-structure for the mantle and density constraints form the Gocid, *Bull. d'Inform. Marees Terr.*, **108,** 7775–7792.

Scherneck, H.G., 1991. A parametrized solid earth tide model and ocean loading effects for global geodetic baseline measurements, *Geophys. J. Int.*, **106,** 677–694.

Schwiderski, E.W., 1980. On charting global ocean tides, *Rev. Geophys. Space Phys.*, **18,** 243–268.

Shimada, S., 1978. Semidiurnal and diernal variations in earthquake swarm activity in the Izu Peninsula during the period from 1975 to 1978, *Bull. Earthq. Res. Inst.*, **53,** 815–822 (in Japanese).

Shlien, S., 1972. Earthquake-tide correlation, *Geophys. J. R. astr. Soc.*, **28,** 27–34.

Shlien, S. & Toksöz, M.N., 1970. A clustering model for earthquake occurrences, *Bull. seism. Soc. Am.*, **60,** 1765–1787.

Souriau, M., Souriau, A. & Gagnepain, J., 1982. Modeling and detecting interactions between earth tides and earthquakes with application to an aftershock sequence in Pyrenees, *Bull. seism. Soc. Am.*, **72,** 165–180.

Takeuchi, H. & Saito, M., 1972. Seismic surface waves, in *Methods in Computational Physics*, Vol. II, pp. 217–295, Academic Press, New York.

Tanaka, T., 1985. Earth tide and earthquakes, in *Earthquake Prediction*, Vol II, pp. 287–307, eds Abe, K., Rikitake, T., Sato, R. & Hagiwara, Y., Center for Academic Publications Japan, Tokyo (in Japanese).